Journal of Advanced Ceramics
2018, **7**(3): 197–206
https://doi.org/10.1007/s40145-018-0271-7
ISSN 2226-4108
CN 10-1154/TQ

Research Article

N-doped graphene and TiO_2 supported manganese and cerium oxides on low-temperature selective catalytic reduction of NO_x with NH_3

Chunlin ZHAO[a,*], Yanxia WU[a], Hailong LIANG[a], Xi CHEN[a], Jie TANG[a], Xianzhong WANG[b,c]

[a]*Institute of Ceramic Science, China Building Material Academy, Beijing, China*
[b]*Department of Materials Science and Engineering, Pingxiang College, Jiangxi, China*
[c]*Jiangxi Province Building Materials Industry Catalyst and Carrier Engineering Technology Research Center, Jiangxi, China*

Received: December 08, 2017; Revised: March 18, 2018; Accepted: March 19, 2018

Abstract: A series of N-doped graphene (NG) and TiO_2 supported MnO_x–CeO_2 catalysts were prepared by a hydrothermal method. The catalysts with different molar ratios of Mn/Ce (6∶1, 10∶1, 15∶1) were investigated for the low-temperature selective catalytic reduction (SCR) of NO_x with NH_3. The synthesized catalysts were characterized by HRTEM, SEM, XRD, BET, XPS, and NH_3-TPD technologies. The characterization results indicated that manganese and cerium oxide particles dispersed on the surface of the TiO_2–NG support uniformly, and that manganese and cerium oxides existed in different valences on the surface of the TiO_2–NG support. At Mn element loading of 8 wt%, MnO_x–CeO_2(10∶1)/TiO_2–1%NG displayed superior activity and improved SO_2 resistance. On the basis of the catalyst characterization, excellent catalytic performance and SO_2 tolerance at low temperature were attributed to the high content of manganese with high oxidation valence, extensive oxidation of NO into NO_2 by CeO_2 and strong NO adsorption capacity, and electron transfer of N-doped graphene.

Keywords: low-temperature; selective catalytic reduction (SCR); N-doped grapheme (NG); manganese and cerium oxides

1 Introduction

Nitrogen oxides (NO_x) are one of the main atmospheric pollutants, which have given rise to a variety of health-related and environmental issues [1–3]. The environmental effects of nitrogen oxides (NO_x) include formation of photochemical smog, acid precipitation, greenhouse effect, ozone depletion, and fine particles. Selective catalytic reduction (SCR) is most widely used in flue gas denitrification technology. The reaction mechanism of SCR technique is that the reducing agent (usually NH_3) selectively reduces NO_x to N_2 under the action of the catalyst in an oxygen-containing atmosphere. In recent years, low-temperature selective catalytic reduction (SCR) with NH_3 is a promising method to remove NO_x in flue gas because the catalyst unit can be located downstream of the particulate control device and desulfurization system, where the temperature is declined to 120–180 ℃ [4–6]. Mn-based catalysts

* Corresponding author.
E-mail: zhaochunlin@cbmamail.com.cn

exhibit excellent $DeNO_x$ activity at low temperature of 80–220 ℃, such as MnO_x–CeO_2/TiO_2, MnO_x–FeO_x/TiO_2, and so on [7–11]. Because manganic oxides have a variety of different surface active oxygen, they can be used to complete the catalytic cycle. But SO_2 in the exhaust gas could easily lead to serious poisoning effect on SCR catalytic in the low-temperature range [12,13]. Ce-based NH_3-SCR catalysts have also been widely studied due to the high oxygen storage capacity and excellent redox properties of CeO_2 [14–16]. Therefore, low-temperature SCR catalysts with high activity and good SO_2 resistance have obtained wide concern [17,18].

In the past years, graphene has drawn an amount of attention as a promising candidate for wide applications in catalysis due to unique two-dimensional monolayer structure, and physical and chemical properties [19–22]. It has a large specific surface area, high electron mobility, and high stability, and is widely used in the study of heterogeneous catalyst support [23–28]. The graphene-supported catalytic system exhibits many special catalytic activities. By introducing graphene into the catalyst, the loading of the active component (MnO_x) is improved, and hence the catalytic activity is enhanced [6]. Some researches indicated that incorporation of nitrogen into the carbon structures enhances the SCR activity [29,30]. N element can be doped through post treatment of graphene or GO, such as hydrazine reduction, and thermal annealing in ammonia method [31–33]. It has been well established that the incorporation of N atoms into the graphene matrix can lead to three main types of N formats, including graphitic N with direct substitution structure, and pyridinic N and pyrrolic N structures [34]. Through the surface functionalization to form a controllable chemical defect, the special physical and chemical properties of N-doped graphene play a role in increasing the active site of the supported catalyst. The pyridine-like N is absorbing nitric oxide (NO) more easily than the graphite-like N [35]. It has been discovered and reported that N-doped graphene can be used as a new catalyst for the oxygen reduction reaction [36], C–H bond activation reaction [37], reduction of nitro compounds [38], oxidation of benzylic alcohols [39], and electrochemical biosensing [40]. However, there is few report about N-doped graphene for SCR reactions.

We recently found that the hydrothermal synthesis method has the advantages of simplicity, high efficiency, high purity, and good homogeneity. The Mn–Ce–Ti mixed oxide catalyst prepared by the hydrothermal method exhibited excellent NH_3-SCR activity and strong resistance against H_2O and SO_2 with a broad operating temperature window [41]. The purpose of this work is to study the effect of NH_3-SCR on the removal of NO_x in flue gas at low temperature and to develop low-temperature SCR denitrification catalyst with high activity and high durability with MnO_x, CeO_x, N-doped grapheme, and TiO_2 as main components. In this work, a series of MnO_x–CeO_2/TiO_2–1%NG catalysts were prepared by the hydrothermal method, which few researchers have concerned about. To fully examine the structure and catalytic mechanism, the catalysts were characterized by SEM, HRTEM, XRD, BET, NH_3-TPD, and XPS.

2 Experimental

Expandable graphite (50 mesh) was supplied by Qingdao Tianhe Graphite Co., Ltd. Manganous nitrate (50% solution), and cerium (Ⅲ) nitrate hexahydrate ($Ce(NO_3)_3·6H_2O$, 99.0%) were purchased from Sinopharm Chemical Reagent Co., Ltd. (Beijing, China). Sodium nitrate ($NaNO_3$, 99.0%), urea (H_2NCONH_2, 99.0%), and ammonia solution (NH_3, 25%–28%) were purchased from Modern Oriental (Beijing) Technology Development CD., Ltd. Potassium permanganate ($KMnO_4$, 99.3%), hydrogenperoxide (H_2O_2, 30%), sulfuric acid (H_2SO_4, 97%), hydrochloricacid (HCl, 36.5%–38%), and titanium dioxide (TiO_2, 98.5%) were purchased from Beijing Chemical Reagent Company. All of the chemical reagents were of analytical grade and used as received without further purification. All aqueous solutions were prepared using deionized water.

2. 1 Preparation of graphene oxide (GO)

GO is obtained by chemical oxidation treatment, which is synthesized by a pressurized oxidation [42]. Graphite, $KMnO_4$, sulphuric acid (98%), and a Teflon reactor were completely cooled in a refrigerator at 0–4 ℃ before use. The Teflon reactor was placed in a stainless steel autoclave. The cooled graphite (2 g) and $KMnO_4$ (8 g) were put into the reactor, and then, sulphuric acid (60 mL) was added. As soon as the sulphuric acid was added, the reactor and stainless steel autoclave were covered and fasten down. The autoclave was kept at 0–4 ℃ for 1.5 h and then heated at 100 ℃ in an oven for 1.5 h. The obtained mud was diluted with 1 L

water. With mechanical stirring, H_2O_2 (30%) was dripped into the suspension until the slurry turned golden yellow. The suspension was washed with hot HCl and deionized water until the pH reached 7, and humid graphite oxide was obtained. After drying, 1 g of GO was added under stirring to 1 L of deionized water. The suspension was placed in an ultrasonic bath for 3 h and then centrifuged at 4000 rpm. The supernatant, consisting of a dispersion of GO with a concentration of about 1 mg/mL, was finally recovered and used for the N-doped graphene preparation.

2. 2 Preparation of N-doped graphene (NG)

0.9 g of urea was added to 60 mL of GO dispersion under magnetic stirring for 30 min. The mass ratio of GO to urea was 1 ∶ 30 [43]. The suspension was placed in autoclave at 160 ℃ for 3 h, and then washed several times. The precipitation was dried. Finally, the product was tagged as NG.

2. 3 Synthesis of catalyst

The MnO_x–CeO_2/TiO_2–1%NG catalysts were prepared with different molar ratios of Mn/Ce by the hydrothermal method. Mn element accounted for 8 wt% of catalyst quality. Appropriate amounts of $Mn(NO_3)_2$, $Ce(NO_3)_3 \cdot 6H_2O$, NG, and TiO_2 were dissolved in deionized water at room temperature and stirred for 20 min, and then ammonia solution (25 wt%, 20 mL) was slowly added to the above solution under vigorous stirring until pH = 11 was achieved. After stirring for 30 min, the obtained suspension was transferred to a 250 mL Teflon-sealed autoclave and allowed to react at 130 ℃ for 12 h. The precipitate was separated by centrifugation and washed several times with deionized water and ethanol, respectively. The resulting powder was dried at 100 ℃ for 12 h, and then calcined in a tubular furnace in a nitrogen atmosphere at 450 ℃ for 3 h. For comparison, MnO_x–CeO_2/TiO_2 and MnO_x/TiO_2–1%NG were also prepared by the same preparation method as described above.

2. 4 Catalyst characterization

The morphology of the samples was characterized by scanning electron microscopy (SEM; Quanta 250 FEG, FEI, USA), and high-resolution transmission electron microscopy (HRTEM; JEM-2100, JEOL, Japan). The structure of the samples was determined by X-ray diffraction (XRD) performed on a Bruker D8 Advance diffractometer, running at 60 kV and 30 mA. The specific surface areas were calculated from adsorbed nitrogen volume by an automatic volumetric apparatus following standard Brunauer–Emmett–Teller (BET) theory, with a Micromeritics ASSP2020 equipment by N_2 physisorption at 77 K. Temperature-programmed desorption of NH_3 (NH_3-TPD) was conducted using a TP5080 auto-adsorption apparatus (XQ, Tianjin). The catalysts (150 mg) were pretreated at 300 ℃ in a flow of N_2 (30 mL/min) for 0.5 h and cooled to 100 ℃ under N_2 flow. Then the samples were exposed to a flow of NH_3 at 100 ℃ for 1 h, followed by N_2 purging for 0.5 h. Finally, the reactor temperature was raised to 600 ℃ under N_2 flow at a constant rate of 10 ℃/min. The X-ray photoelectron spectroscopy (XPS) was carried out to analyze surface chemical composition and the valence state of the metal species on the surface of the catalysts on an Escalab 250 xi spectrometer (Thermo, USA) with Al Kα radiation source, and the binding energy was corrected using the C 1s spectrum at 284.8 eV.

2. 5 SCR performance test

SCR activity measurement was performed in a fixed-bed reactor using the catalyst of 40–60 mesh at 100–200 ℃ by ZHKPR Instrument Co., Ltd. (Chengdu, China). The reactor was placed in an electrically heated furnace with the typical reaction gas consisted of 500 ppm NO, 500 ppm NH_3, 6 vol% O_2, 100 ppm SO_2 (when used), balance N_2 gas, and GHSV = 30000 h^{-1}. The inlet and outlet concentrations of NO_x were continually measured by an analyzer (Testo 350, Germany). All the data were obtained after 20 min as the SCR reaction reached steady state. NO_x conversion was calculated according to the following formula:

$$\text{NO}_x \text{ conversion } (\%) = \frac{[\text{NO}_x]_{\text{in}} - [\text{NO}_x]_{\text{out}}}{[\text{NO}_x]_{\text{in}}} \times 100$$

where $[NO_x]_{in}$ and $[NO_x]_{out}$ represent the inlet and outlet concentrations of NO_x under steady-state status, respectively.

3 Results and discussion

3. 1 Morphology and texture

The TEM image in Fig. 1(a) shows that N-doped graphene is transparent with some clearly visible wrinkles, suggesting that NG is mainly composed of few layers. Because the sheets have a high specific

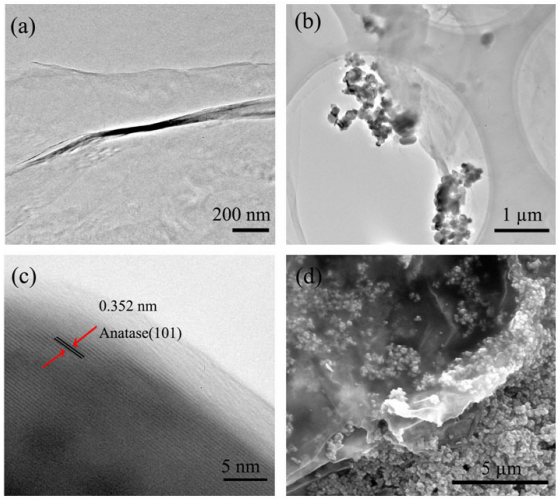

Fig. 1 (a) TEM image of NG; (b) TEM and (c) HRTEM images of MnO_x–CeO_2/TiO_2–1%NG; (d) SEM image of MnO_x–CeO_2/TiO_2–1%NG.

surface area, in order to reduce the surface energy, there will be overlapping phenomenon. Figure 1(b) shows the TEM image of the MnO_x–CeO_2/TiO_2–1%NG catalyst at a Mn/Ce molar ratio of 10:1. It is clear that a large number of TiO_2 nanoparticles ranging from 100 to 200 nm with an average particle size of *ca*. 150 nm, are anchored onto the stacked and wrinkled NG sheets. The corresponding HRTEM image reveals clear lattice fringes. Figure 1(c) shows the fringe spacing is 0.352 nm, corresponding to the (101) plane of anatase TiO_2. The low-magnification SEM image in Fig. 1(d) indicates that MnO_x–CeO_2 and TiO_2 nanoparticles are anchored onto the surface of NG sheets and some particles aggregate together. A large amount of the catalyst nanoparticles uniformly disperse on the surface of the N-doped graphene carrier and the surface area of the MnO_x–CeO_2/TiO_2–1%NG catalyst is greatly increased.

3.2 GO and NG by XPS

In order to investigate the effect of urea on GO reduction and nitrogen doping in hydrothermal process, XPS was used to qualitatively and quantitatively analyze the samples. It can be seen from the XPS full spectra (Fig. 2(a)) that the intensity of the O 1s (531.3 eV) peak is significantly reduced after the hydrothermal reaction, indicating that GO is reduced. N 1s (~399.3 eV) peak of NG is also observed indicating that nitrogen element is doped into the sample, and N element content is up to 6.33% as shown in Table 1. C=C (284.6 eV), C–O/C–O–C (286.9 eV), and C=O (288.2 eV) are found in the C 1s XPS spectra of GO (Fig. 2(b)) and NG (Fig. 2(c)). After hydrothermal process, the content of C–O (286.9 eV) is significantly reduced in NG (Fig. 2(c))

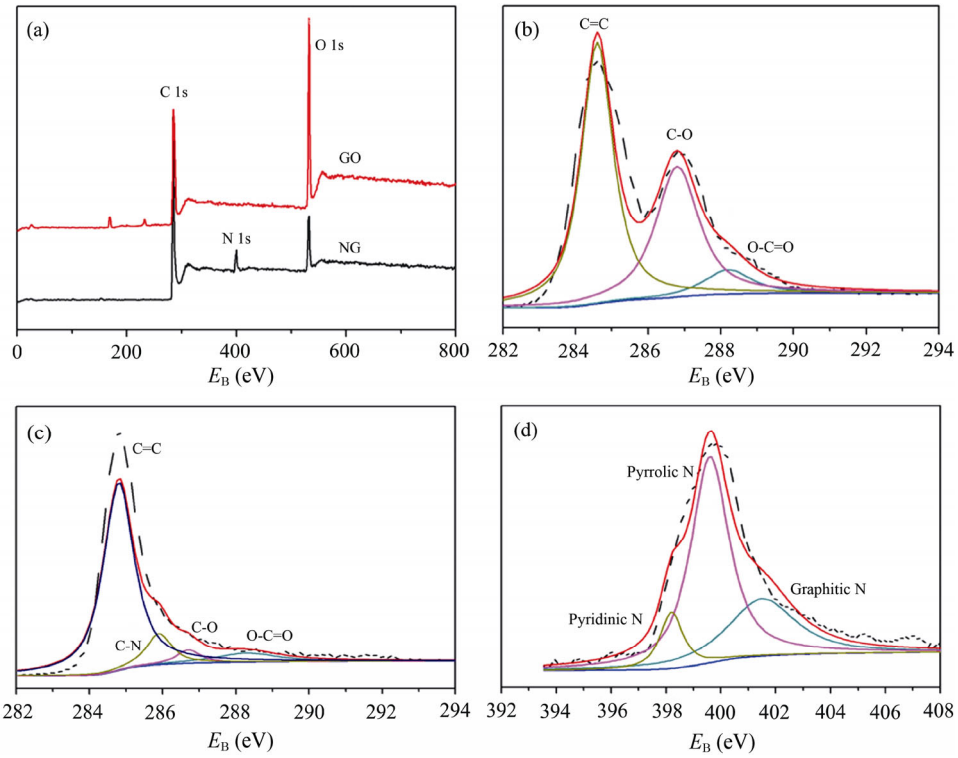

Fig. 2 (a) XPS full spectra of GO and NG; (b) and (c) high-resolution C 1s XPS spectra of GO and NG respectively; (d) high-resolution N 1s XPS spectrum.

compared to that in GO (Fig. 2(b)), which indicates GO is reduced with urea. A C–N peak (285.9 eV) is appeared (Fig. 2(c)). N atoms are divided into "pyridinic N" (398.2 eV), "pyrrolic N" (399.5 eV), and "graphitic N" (401.5 eV) as shown in Fig. 2(d), which replace the C atoms in the graphene lattice [43]. Nitrogen atoms of NG due to its basic nature should have affinity towards weakly acidic molecules like NO. The presence of nitrogen in the carbon matrix was reported to enhance adsorption of NO [29,35], which may cause an electron transfer from the support surface to the NO molecules. Table 1 lists the surface atomic concentrations of GO and NG. Consequently, GO is reduced with urea after the removal of a large number of oxygenated functional groups, and nitrogen element is doped into the graphene lattice.

3. 3 XRD analysis of the catalysts

Figure 3 shows the XRD patterns of the MnO_x–CeO_2(10:1)/TiO_2–1%NG, MnO_x–CeO_2(10:1)/TiO_2, and TiO_2–1%NG. All diffraction peaks could be readily indexed to anatase TiO_2 (JCPDS Card No. 21-1272). Anatase TiO_2 presents an abundance of active sites, which can enhance the SCR activity of the catalyst. Peaks at 2θ values of 25.3°, 37.8°, 48.1°, 53.9°, 55.0°, 62.7°, 68.7°, 70.3°, and 75.1° are respectively indexed to the (101), (004), (200), (105), (211), (204), (116), (220), and (215) crystal planes of anatase TiO_2 [26].

Table 1 C, N, O surface atomic concentrations of GO and NG

Sample	Atomic composition (%)		
	C	O	N
GO	66.73	30.14	1.66
NG	82.27	11.39	6.33

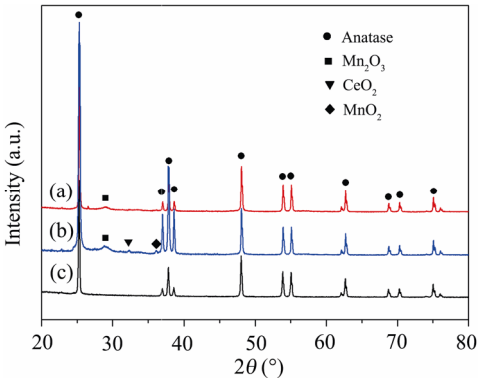

Fig. 3 XRD patterns of (a) MnO_x–CeO_2/TiO_2–1%NG, (b) MnO_x–CeO_2/TiO_2, and (c) TiO_2–1%NG.

The diffraction peaks of MnO_x are characteristic of Mn_2O_3 (JCPDS Card No. 06-0540) in MnO_x–CeO_2(10:1)/TiO_2–1%NG and MnO_x–CeO_2(10:1)/TiO_2 peaks at 2θ values of 28.9°. The weak diffraction peaks at 33.1° can be attributed to ceria with a cubic fluorite structure (JCPDS Card No. 34-0394), and the weak diffraction peaks at 37.1° can be attributed to MnO_2 (JCPDS Card No. 30-0820) [6]. The above two peaks have only been found in MnO_x–CeO_2(10:1)/TiO_2. Furthermore, the peak intensities of MnO_x–CeO_2(10:1)/TiO_2–1%NG are lower than those of MnO_x–CeO_2(10:1)/TiO_2, indicating that the addition of NG results in the lower crystallinity of MnO_x–CeO_2. However, characteristic diffraction peaks for MnO_x and CeO_2 are not obvious in the MnO_x–CeO_2(10:1)/TiO_2–1%NG and MnO_x–CeO_2(10:1)/TiO_2 because of the amorphous nature [45].

3. 4 BET surface area and pore size distribution

Detailed data of the specific surface area, pore volume, and pore size of MnO_x–CeO_2/TiO_2 and MnO_x–CeO_2/TiO_2–1%NG are listed in Table 2. Through adding NG, MnO_x–CeO_2/TiO_2–1%NG has a larger specific surface area than MnO_x–CeO_2/TiO_2, which leads to the high dispersion in the metal oxide composite with the support. The nitrogen adsorption–desorption isotherms are displayed in Fig. 4. According to the Brunauer–Deming–Deming–Teller (BDDT) classification, the majority of physisorption isotherms could be classified into six types. As shown in Fig. 4, MnO_x–CeO_2/TiO_2 and MnO_x–CeO_2/TiO_2–1%NG could both be classified into the representative type IV adsorption–desorption isotherm with an H3-type hysteresis loop [6]. The samples have mesoporous structure, which could be derived from the packing of the nanoparticles. MnO_x–CeO_2/TiO_2–1%NG presents larger pore volume than MnO_x–CeO_2/TiO_2. As illustrated in Table 2, the pore distribution of MnO_x–CeO_2/TiO_2 and MnO_x–CeO_2/TiO_2–1%NG shows an average pore size of 13.20 and 13.03 nm, respectively. In general, the larger specific surface area is expected to be beneficial to offer more active sites and increase the adsorption of reactants in

Table 2 Porous structure parameters of MnO_x–CeO_2/TiO_2 and MnO_x–CeO_2/TiO_2–1%NG catalysts

Catalyst	BET surface area (m^2/g)	Pore volume ($10^{-2}cm^3$/g)	Average pore diameter (nm)
MnO_x–CeO_2/TiO_2	44.9342	14.8252	13.20
MnO_x–CeO_2/TiO_2–1%NG	58.8247	19.1714	13.03

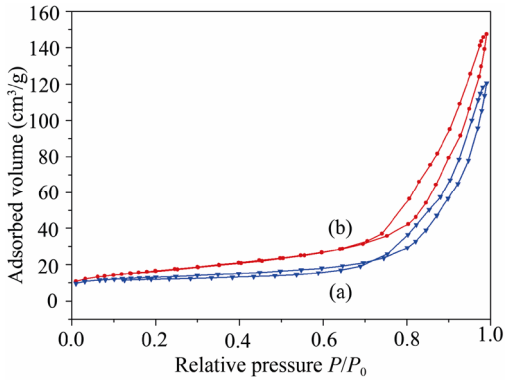

Fig. 4 Nitrogen adsorption–desorption isotherms of the catalysts: (a) MnO_x–CeO_2/TiO_2 and (b) MnO_x–CeO_2/TiO_2–1%NG.

the catalytic reaction, resulting in the excellent catalytic performance of MnO_x–CeO_2/TiO_2–1%NG.

3. 5 Chemical composition by XPS

To obtain the information on the atomic concentration and element chemical state of manganese or cerium species in the catalysts, the surface of samples was further investigated by XPS. Figure 5 illustrates the XPS spectra of Mn 2p, Ce 3d, and O 1s. The atomic surface compositions of MnO_x–CeO_2/TiO_2, fresh and spent MnO_x–CeO_2/TiO_2–1%NG have been summarized by XPS in Table 3. Results show that MnO_2 and MnO/Mn contents of the spent catalyst increase relative to those in the fresh catalyst. N element content of the spent catalyst slightly reduces relative to the fresh catalyst. As shown in Fig. 5(a), peak-fitting deconvolution separates the Mn $2p_{3/2}$ spectra into three characteristic peaks attributed to Mn^{2+} (640.8 eV), Mn^{3+} (641.8 eV), and Mn^{4+} (643.4 eV). The Mn $2p_{1/2}$ spectra show two peaks at 653.88 eV (Mn^{4+}) and 653.0 eV (MnO_x/Mn) [26]. The presence of multiple-valence manganese oxides contributes to the oxidation–reduction reaction. Furthermore, the relative surface content of manganese oxides with different valences also changes, which plays an important role in improving the electron transfer and low-temperature SCR activity of MnO_x–CeO_2/TiO_2–1%NG catalysts. It is noted that the relative surface content of Mn^{4+} (Mn^{4+}/Mn) over MnO_x–CeO_2/TiO_2–1%NG (37.9%) is much higher than that over MnO_x–CeO_2/TiO_2 (32.6%). It is clear that much more Mn^{4+}/Mn species are exposed on the surface of MnO_x–CeO_2/TiO_2–1%NG, while the Mn^{4+} species and their redox cycle might be beneficial for the high activity in the NH_3-SCR reaction at low temperature, attributed to the enhancement of NO reduction to N_2. Active components are highly dispersed on the surface of the catalyst support by introduction of NG, which affects the surrounding electronic state of manganese species, may also explain the improvements in SCR activity observed in this work.

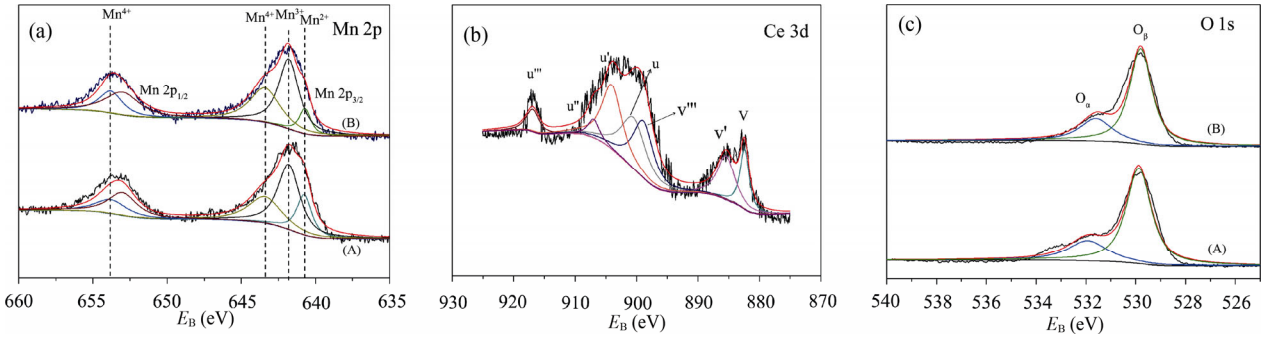

Fig. 5 XPS spectra for (a) Mn 2p, (b) Ce 3d, and (c) O 1s of the catalysts: (A) MnO_x–CeO_2/TiO_2 and (B) MnO_x–CeO_2/TiO_2–1%NG.

Table 3 Atomic surface compositions of MnO_x–CeO_2/TiO_2 and MnO_x–CeO_2/TiO_2–1%NG(fresh, spent) obtained by XPS

Sample	Atomic composition (%)											
	C	N	Mn	Ce	Ti	O	O		Mn			
							O_α	O_β	MnO/Mn	Mn_2O_3/Mn	MnO_2/Mn	MnO_x/Mn
MnO_x–CeO_2/TiO_2	—	—	4.2	2.3	39.5	54.0	14.8	39.2	0.151	0.358	0.326	0.165
MnO_x–CeO_2/TiO_2–1%NG (fresh)	9.5	0.5	4.6	2.5	25.6	57.3	16.3	41.0	0.073	0.352	0.379	0.196
MnO_x–CeO_2/TiO_2–1%NG (spent)	9.2	0.4	4.7	2.4	25.3	58.0	16.7	41.3	0.080	0.350	0.382	0.188

The Ce 3d spectrum is presented in Fig. 5(b). The peaks are attributed to $3d_{3/2}$ and $3d_{5/2}$ spin-orbit states. The peaks at the binding energy of 882.4 (v), 898.9 (v'''), 900.5 (u), 907 (u''), 916.9 (u''') eV are assigned to Ce^{4+}. The peaks at the binding energy of 885.4 (v') and 904.5 (u') are assigned to Ce^{3+} species [6]. Results imply that Ce^{4+} is the main valence state in MnO_x–CeO_2/TiO_2–1%NG catalyst. No obvious difference is observed from the Ce 3d XPS spectra of MnO_x–CeO_2/TiO_2 and MnO_x–CeO_2/TiO_2–1%NG samples.

The XPS patterns of O 1s (Fig. 5(c)) show the presence of two types of surface oxygen in the samples. The peak at 529.4–529.7 eV corresponds to lattice oxygen (O_β), while that at 531.6–532.0 eV is assigned to chemisorbed oxygen (O_α, surface-adsorbed oxygen), such as O_2^{2-} or O^-, in the form of OH^- and CO_3^{2-} [26]. According to the XPS analysis, the surface concentration of O_α species on MnO_x–CeO_2/TiO_2–1%NG is higher than that on MnO_x–CeO_2/TiO_2. It has been demonstrated that O_α species are more active than O_β species, due to their higher mobility [46]. Hence, the higher concentration of O_α species is beneficial to the NH_3-SCR of NO, resulting in the promotion of the reduction of NO and the subsequent facilitation of the "fast SCR" reaction.

3. 6 Acidic properties

The adsorption and activation of NH_3 at active sites of the catalysts play an important role in the NH_3-SCR reaction. NH_3-TPD was performed to investigate the surface acid amount and strength of the catalysts, and the corresponding results are shown in Fig. 6(b). The area and position of these desorption peaks directly relate to the amounts of acidic sites and their acidic strength, respectively. One broad peak spanning the temperature range of 100–250 ℃ is observed for both samples, attributed to physisorbed NH_3 and NH_3 at weak acid sites. The NH_3-TPD physisorption is too weak to activate NH_3 molecules, while the adsorbed NH_3 species on strong acid sites are hardly to desorb, which make not much contribution to low-temperature NH_3-SCR reaction. Therefore, we focus on the adsorption of NH_3 molecules on medium-strong acid sites. The desorption peak at 306 ℃ of the MnO_x–CeO_2/TiO_2–1%NG is obviously higher than MnO_x–CeO_2/TiO_2 as shown in Fig. 6. It is considered that the peak area correlates with the acid amount. This indicates that MnO_x–CeO_2/TiO_2–1%NG catalysts have more acid sites than MnO_x–CeO_2/TiO_2, which may be due to the increase in specific surface area of MnO_x–CeO_2/TiO_2–1%NG and improve the dispersion of the catalyst nanoparticles. Therefore, MnO_x–CeO_2/TiO_2–1%NG has a stronger acid intensity due to the addition of NG. The difference in the strength and the number of acid sites on the two catalysts might lead to the distinction of their catalytic performances. In other word, MnO_x–CeO_2/TiO_2–1%NG catalyst possesses the largest amount of NH_3 molecules, and further promotes the enhancement of catalytic performance for NH_3-SCR reaction.

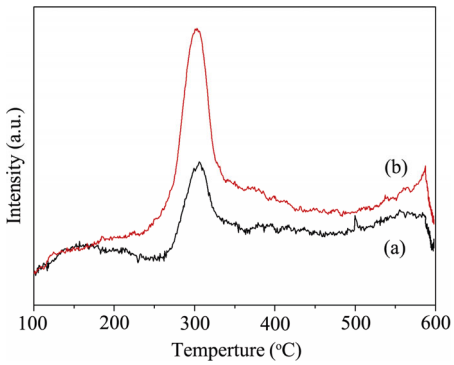

Fig. 6 NH_3-TPD profiles of the catalysts: (a) MnO_x–CeO_2/TiO_2 and (b) MnO_x–CeO_2/TiO_2–1%NG.

3. 7 Catalytic activity

Figure 7 shows the NH_3-SCR activity of these prepared catalysts with the variation in temperature. It can be seen that the NO_x conversion over all the catalysts increases with increasing temperature in 80–200 ℃. The loading of manganese element is 8 wt%, together with different molar cerium supported on TiO_2–1%NG. When the Mn/Ce molar ratio is 10 : 1, the NO_x conversion is up to 99% at 160 ℃. Further when the Mn/Ce molar ratio is 6 : 1, NO_x conversion decreases evidently. MnO_x–CeO_2(10 : 1)/TiO_2–1%NG samples have higher SCR activity compared to MnO_x/TiO_2–1%NG in the temperature region. It also can be seen that the MnO_x–CeO_2(10 : 1)/TiO_2–1%NG samples have higher SCR activity compared to MnO_x–CeO_2 (10 : 1)/TiO_2 in the whole temperature region. The reaction mechanism may be gaseous NH_3 molecules are adsorbed onto the acid sites to form NH_4^+ ions, and then the formed molecules of NO_2 react with adjacent NH_4^+ ions to produce N_2 and H_2O [29]. Nitrogen atoms of NG as a basic center can adsorb acid gas NO and the increased adsorption may be associated with an electron transfer between the support surface to the NO molecule, which is oxidized NO_2. The reaction is probably the rate-determining step for SCR reaction of catalysts. This demonstrates that NG improves

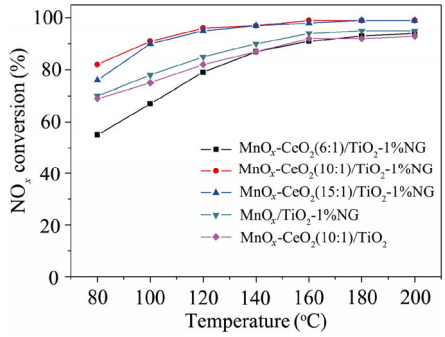

Fig. 7 NH_3-SCR performance of the catalysts. Reaction conditions: 500 ppm NO, 500 ppm NH_3, 6% O_2, and balance N_2, GHSV = 30000 h^{-1}.

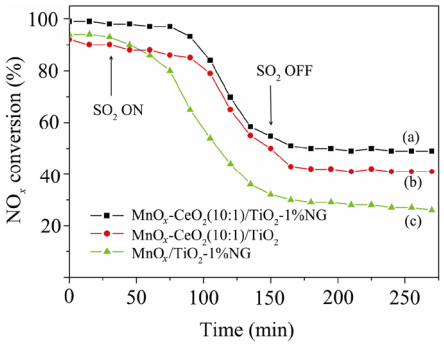

Fig. 8 SO_2 tolerance of (a) MnO_x–CeO_2(10 : 1)/TiO_2–1%NG, (b) MnO_x–CeO_2(10 : 1)/TiO_2, and (c) MnO_x/TiO_2–1%NG at 160 ℃. Reaction conditions: 500 ppm NO, 500 ppm NH_3, 6% O_2, 100 ppm SO_2, and balance N_2, GHSV = 30000 h^{-1}.

interaction of the species, which possibly provides more effective contact with the reactants resulting in the process of NO adsorption oxidation.

3. 8 Influence of SO_2

The SO_2 resistance effects of the catalysts on NO_x conversion at 160 ℃ are investigated in Fig. 8. It is obvious that the NG in MnO_x–CeO_2/TiO_2–1%NG plays a great role in the high catalytic activity. It shows that when 100 ppm SO_2 is added to the system, the NO_x conversion of MnO_x–CeO_2(10 : 1)/TiO_2–1%NG decreases from an initial value of 99% to 55% in 2 h. And when SO_2 is removed from the flue gas, the activity of MnO_x–CeO_2(10 : 1)/TiO_2–1%NG reaches a stable level of about 49%. For MnO_x–CeO_2/TiO_2 resistance to SO_2, SCR reaction system was also studied and a similar phenomenon is observed. The NO_x conversion markedly decreases to 50% in 2 h and is finally restored to 41%. For MnO_x/TiO_2–1%NG resistance to SO_2, the NO_x conversion markedly decreases to 32% in 2 h and is finally restored to 26%. These indicate that the NO_x conversion of MnO_x–CeO_2/TiO_2–1%NG obviously decreases but a relatively higher activity is still maintained compared with MnO_x–CeO_2/TiO_2 and MnO_x/TiO_2–1%NG. The results indicate that introduction of NG and Ce enhances the resistance of Mn-based catalysts to SO_2. A possible reason is that nitrogen functional group of NG due to its basic nature can absorb acid gas SO_2. Consequently, NG can act as a SO_2 trap to limit the sulfation of the main active phase when exposed to SO_2. Introduction of Ce inhibits the formation of manganese sulfates, lowers the probability of surface active site poisoning by SO_2, and decreases by-products, such as NH_4SO_3 and NH_4HSO_4, all of which could improve the resistance of the catalyst to SO_2 poisoning during low-temperature SCR.

4 Conclusions

In summary, a series of MnO_x–CeO_2/TiO_2–1%NG catalysts were successfully prepared with different molar ratios of Mn/Ce by the hydrothermal method. The obtained results of HRTEM images and XRD patterns showed the anatase TiO_2 and several valences of amorphous manganese and cerium oxides were uniformly distributed on the surface of the catalysts. Among the catalysts prepared, MnO_x–CeO_2(10:1)/TiO_2–1%NG catalyst exhibited the highest SCR activity (up to 99% at 160 ℃). MnO_x was observed as MnO, MnO_2, Mn_2O_3, and non-stoichiometric MnO_x/Mn in the samples by XPS. Redox reactions were likely to occur in the presence of manganese oxides with multiple valence states. The introduction of NG could be associated with the high specific surface areas, which provided more active sites to adsorb and activate reagents. In particular, active sites on the surface of NG adsorb NO molecular. Addition of Ce increased chemisorbed oxygen on the catalyst surface and promoted NO oxidation into NO_2, thereby improving the redox performance of the catalyst. MnO_x–CeO_2(10:1)/TiO_2–1%NG exhibited a large surface area, high activity, and improved resistance to SO_2 at low temperatures. This work enhanced the low-temperature NH_3-SCR performance and SO_2 tolerance of catalysts by adding NG and promoted the practical application of these catalysts in low-temperature SCR.

Acknowledgements

This project is financially supported by the Program of

Frontier Exploration Fund of China Building Materials Academy, "the whole process of air pollution control on new technology research" (No. 2016YFC0209302).

References

[1] Kim CH, Qi G, Dahlberg K, *et al*. Strontium-doped perovskites rival platinum catalysts for treating NO_x in simulated diesel exhaust. *Science* 2010, **327**: 1624–1627.

[2] Xiong ZB, Wu C, Hu Q, *et al*. Promotional effect of microwave hydrothermal treatment on the low-temperature NH_3-SCR activity over iron-based catalyst. *Chem Eng J* 2016, **286**: 459–466.

[3] Parks II JE. Less costly catalysts for controlling engine emissions. *Science* 2010, **327**: 1584–1585.

[4] Liu Z, Li Y, Zhu T, *et al*. Selective catalytic reduction of NO_x by NH_3 over Mn-promoted V_2O_5/TiO_2 catalyst. *Ind Eng Chem Res* 2014, **53**: 12964–12970.

[5] Jin R, Yue L, Wu Z, *et al.* Low-temperature selective catalytic reduction of NO with NH_3 over Mn–Ce oxides supported on TiO_2 and Al_2O_3: A comparative study. *Chemosphere* 2010, **78**: 1160–1166.

[6] Xiao X, Sheng Z, Yang L, *et al.* Low-temperature selective catalytic reduction of NO_x with NH_3 over a manganese and cerium oxide/graphene composite prepared by a hydrothermal method. *Catal Sci Technol* 2016, **6**: 1507–1514.

[7] Andreoli S, Deorsola FA, Pirone R. MnO_x–CeO_2 catalysts synthesized by solution combustion synthesis for the low-temperature NH_3-SCR. *Catal Today* 2015, **253**: 199–206.

[8] Hong J, Pan W, Guo R, *et al*. The effect of iron doping on the performance of Mn/TiO_2 catalysts for NO reduction with NH_3 at low temperature. *Adv Mater Res* 2014, **864–867**: 1415–1420.

[9] Deng S, Meng T, Xu B, *et al*. Advanced MnO_x/TiO_2 catalyst with preferentially exposed anatase {001} facet for low-temperature SCR of NO. *ACS Catal* 2016, **6**: 5807–5815.

[10] Liu Z, Yi Y, Zhang S, *et al*. Selective catalytic reduction of NO_x, with NH_3, over Mn–Ce mixed oxide catalyst at low temperatures. *Catal Today* 2013, **216**: 76–81.

[11] Liu Z, Liu Y, Li Y, *et al.* WO_3 promoted Mn–Zr mixed oxide catalyst for the selective catalytic reduction of NO_x with NH_3. *Chem Eng J* 2016, **283**: 1044–1050.

[12] Ettireddy PR, Ettireddy N, Mamedov S, *et al*. Surface characterization studies of TiO_2 supported manganese oxide catalysts for low temperature SCR of NO with NH_3. *Appl Catal B: Environ* 2007, **76**: 123–134.

[13] Gao F, Tang X, Yi H, *et al*. Promotional mechanisms of activity and SO_2, tolerance of Co- or Ni-doped MnO_x–CeO_2, catalysts for SCR of NO_x with NH_3 at low temperature. *Chem Eng J* 2017, **317**: 20–31.

[14] Liu Z, Yi Y, Li J, *et al*. A superior catalyst with dual redox cycles for the selective reduction of NO_x by ammonia. *Chem Commun* 2013, **49**: 7726–7728.

[15] Shan W, Liu F, He H, *et al*. A superior Ce–W–Ti mixed oxide catalyst for the selective catalytic reduction of NO_x with NH_3. *Appl Catal B: Environ* 2012, **115–116**: 100–106.

[16] Liu Z, Zhang S, Li J, *et al*. Promoting effect of MoO_3 on the NO_x reduction by NH_3 over CeO_2/TiO_2 catalyst studied with *in situ* DRIFTS. *Appl Catal B: Environ* 2014, **144**: 90–95.

[17] Wu Z, Jin R, Wang H, *et al*. Effect of ceria doping on SO_2 resistance of Mn/TiO_2 for selective catalytic reduction of NO with NH_3 at low temperature. *Catal Commun* 2009, **10**: 935–939.

[18] Zuo J, Chen Z, Wang F, *et al*. Low-temperature selective catalytic reduction of NO_x with NH_3 over novel Mn–Zr mixed oxide catalysts. *Ind Eng Chem Res* 2014, **53**: 2647–2655.

[19] Roy-Mayhew JD, Bozym DJ, Punckt C, *et al*. Functionalized graphene as a catalytic counter electrode in dye-sensitized solar cells. *ACS Nano* 2010, **4**: 6203–6211.

[20] Huo X, Liu J, Wang B, *et al*. A one-step method to produce graphene–Fe_3O_4 composites and their excellent catalytic activities for three-component coupling of aldehyde, alkyne and amine. *J Mater Chem A* 2013, **1**: 651–656.

[21] Sun H, Liu S, Zhou G, *et al*. Reduced graphene oxide for catalytic oxidation of aqueous organic pollutants. *ACS Appl Mater Interfaces* 2012, **4**: 5466–5471.

[22] Navalon S, Dhakshinamoorthy A, Alvaro M, *et al*. Carbocatalysis by graphene-based materials. *Chem Rev* 2014, **114**: 6179–6212.

[23] Song EH, Wen Z, Jiang Q. CO catalytic oxidation on copper-embedded graphene. *J Phys Chem C* 2011, **115**: 3678–3683.

[24] Saner B, Gürsel SA, Yürüm Y. Layer-by-layer polypyrrole coated graphite oxide and graphene nanosheets as catalyst support materials for fuel cells. *Fuller Nanotub Car N* 2013, **21**: 233–247.

[25] Zhou X, Qiao J, Yang L, *et al*. A review of graphene-based nanostructural materials for both catalyst supports and metal-free catalysts in PEM fuel cell oxygen reduction reactions. *Adv Eng Mater* 2014, **4**: 1289–1295.

[26] Lu X, Song C, Jia S, *et al*. Low-temperature selective catalytic reduction of NO_x with NH_3 over cerium and manganese oxides supported on TiO_2–graphene. *Chem Eng J* 2015, **260**: 776–784.

[27] Trapalis A, Todorova N, Giannakopoulou T, *et al*. TiO_2/graphene composite photocatalysts for NO_x removal: A comparison of surfactant-stabilized graphene and reduced graphene oxide. *Appl Catal B: Environ* 2016, **180**: 637–647.

[28] Seifvand N, Kowsari E. Novel TiO_2/graphene oxide functionalized with cobalt complex for significant degradation of NO_x and CO. *RSC Adv* 2015, **5**: 93706–93716.

[29] Szymański GS, Grzybek T, Papp H. Influence of nitrogen

surface functionalities on the catalytic activity of activated carbon in low temperature SCR of NO_x with NH_3. *Catal Today* 2004, **90**: 51–59.

[30] Sousa JPS, Pereira MFR, Figueiredo JL. NO oxidation over nitrogen doped carbon xerogels. *Appl Catal B: Environ* 2012, **125**: 398–408.

[31] Wang R, Wang Y, Xu C, *et al*. Facile one-step hydrazine-assisted solvothermal synthesis of nitrogen-doped reduced graphene oxide: Reduction effect and mechanisms. *RSC Adv* 2013, **3**: 1194–1200.

[32] Li X, Wang H, Robinson JT, *et al*. Simultaneous nitrogen doping and reduction of graphene oxide. *J Am Chem Soc* 2009, **131**: 15939–15944.

[33] Wang X, Li X, Zhang L, *et al*. N-doping of graphene through electrothermal reactions with ammonia. *Science* 2009, **324**: 768–771.

[34] Usachov D, Vilkov O, Grüneis A, *et al*. Nitrogen-doped graphene: Efficient growth, structure, and electronic properties. *Nano Lett* 2011, **11**: 5401–5407.

[35] Lv W, Shi K, Li L, *et al*. Nitrogen-doped multiwalled carbon nanotubes and their electrocatalysis towards oxidation of NO. *Microchim Acta* 2010, **170**: 91–98.

[36] Li Y, Li T, Yao M, *et al*. Metal-free nitrogen-doped hollow carbon spheres synthesized by thermal treatment of poly(*o*-phenylenediamine) for oxygen reduction reaction in direct methanol fuel cell applications. *J Mater Chem* 2012, **22**: 10911–10917.

[37] Gao Y, Hu G, Zhong J, *et al*. Nitrogen-doped sp^2-hybridized carbon as a superior catalyst for selective oxidation. *Angew Chem Int Ed* 2013, **52**: 2109–2113.

[38] Kong X, Sun Z, Chen M, *et al*. Metal-free catalytic reduction of 4-nitrophenol to 4-aminophenol by N-doped graphene. *Energy Environ Sci* 2013, **6**: 3260–3266.

[39] Mahyari M, Shaabani A. Graphene oxide-iron phthalocyanine catalyzed aerobic oxidation of alcohols. *Appl Catal A: Gen* 2014, **469**: 524–531.

[40] Wu P, Du P, Zhang H, *et al*. Microscopic effects of the bonding configuration of nitrogen-doped graphene on its reactivity toward hydrogen peroxide reduction reaction. *Phys Chem Chem Phys* 2013, **15**: 6920–6928.

[41] Liu Z, Zhu J, Li J, *et al*. Novel Mn–Ce–Ti mixed-oxide catalyst for the selective catalytic reduction of NO_x with NH_3. *ACS Appl Mater Interfaces* 2014, **6**: 14500–14508.

[42] Bao C, Song L, Xing W, *et al*. Preparation of graphene by pressurized oxidation and multiplex reduction and its polymer nanocomposites by masterbatch-based melt blending. *J Mater Chem* 2012, **22**: 6088–6096.

[43] Su P, Guo H-L, Peng S, *et al*. Preparation of nitrogen-doped graphene and its supercapacitive properties. *Acta Phys-Chim Sin* 2012, **28**: 2745–2753.

[44] Qi G, Yang RT. Low-temperature selective catalytic reduction of NO with NH_3 over iron and manganese oxides supported on titania. *Appl Catal B: Environ* 2003, **44**: 217–225.

[45] Liu F, He H. Structure-activity relationship of iron titanate catalysts in the selective catalytic reduction of NO_x with NH_3. *J Phys Chem C* 2010, **114**: 16929–16936.

[46] Zhang D, Zhang L, Fang C, *et al.* MnO_x–CeO_x/CNTs pyridine-thermally prepared via a novel *in situ* deposition strategy for selective catalytic reduction of NO with NH_3. *RSC Adv* 2013, **3**: 8811–8819.